Electrochemical lithiation synthesis of nanoporous materials with superior catalytic and capacitive activity

YONG-SHENG HU[1]*, YU-GUO GUO[1]*†, WILFRIED SIGLE[2], SARMIMALA HORE[1], PALANI BALAYA[1] AND JOACHIM MAIER[1]†

[1]Max-Planck-Institut für Festkörperforschung, D-70569 Stuttgart, Germany
[2]Max-Planck-Institut für Metallforschung, D-70569 Stuttgart, Germany
*These authors contributed equally to this work
†e-mail: y.guo@fkf.mpg.de; s.weiglein@fkf.mpg.de

Published online: 13 August 2006; doi:10.1038/nmat1709

Nanoporous materials have attracted great technological interest during the past two decades, essentially due to their wide range of applications: they are used as catalysts, molecular sieves, separators and gas sensors as well as for electronic and electrochemical devices[1–5]. Most syntheses of nanoporous materials reported so far have focused on template-assisted bottom-up processes, including soft templating[6–10] (chelating agents, surfactants, block copolymers and so on) and hard templating[11,12] (porous alumina, carbon nanotubes and nanoporous materials) methods. Here, we exploit a mechanism implicitly occurring in lithium batteries at deep discharge[13–18] to develop it into a room-temperature template-free method of wide applicability in the synthesis of not only transition metals but also metal oxides with large surface area and pronounced nanoporosity associated with unprecedented properties. The power of this top-down method is demonstrated by the synthesis of nanoporous Pt and RuO_2, both exhibiting superior performance: the Pt prepared shows outstanding properties when used as an electrocatalyst for methanol oxidation, and the RuO_2, when used as a supercapacitor electrode material, exhibits a distinctly better performance than that previously reported for non-hydrated RuO_2 (refs 19,20).

Recently, it has been found that in lithium batteries, transition metal oxide (MO_x with M = Cr, Mn, Fe, Co, Ni, Cu, Ru and so on) electrodes can be reversibly discharged down to the metal level at room temperature[13–18]. In these studies, pioneered by the work of Poizot *et al.*[13], it was found that electrochemical lithiation typically leads to *in situ* formation of a M/Li_2O nanocomposite in which nanometre-scale metal clusters are embedded in a Li_2O matrix, accompanied by a large volume expansion (for example, in the cases of PtO_2/RuO_2, the volume expands up to 100% on 4Li insertion) (Fig. 1). The latter can be considered as a possible reason for the evolution of the nanostructure which is further stabilized by the penetration of electrolytes resulting in chemical transport being blocked and preventing further growth of the metal cluster. When the battery is charged and Li is electrochemically extracted from the M/Li_2O nanocomposite, the nanocrystalline transition metal oxide formed can be used as the electrode for subsequent cycles. In this way, a large amount of Li can be reversibly stored in lithium batteries[13–18]. Here, we wish to use such a mechanism to deliberately synthesize nanoporous metals, metal oxides, and their composites, that is, we are not interested in storing Li, rather Li is used as a structure-forming chemical agent which has to be removed at the end of the synthesis, when the nanoporous materials have been obtained. There is only a single very recent report known to us that emphasizes the possibility of using the above method to synthesize nanoparticles[18]. However, Cu nanoparticles thus obtained were not studied further with respect to improved properties or potential applications.

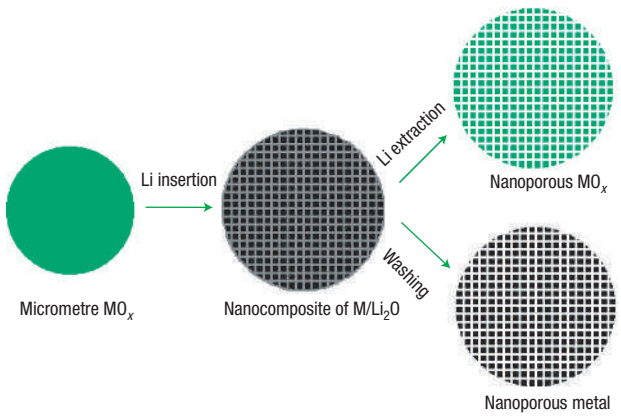

Figure 1 General scheme for the template-free electrochemical lithiation/delithiation synthesis of nanoporous structures.

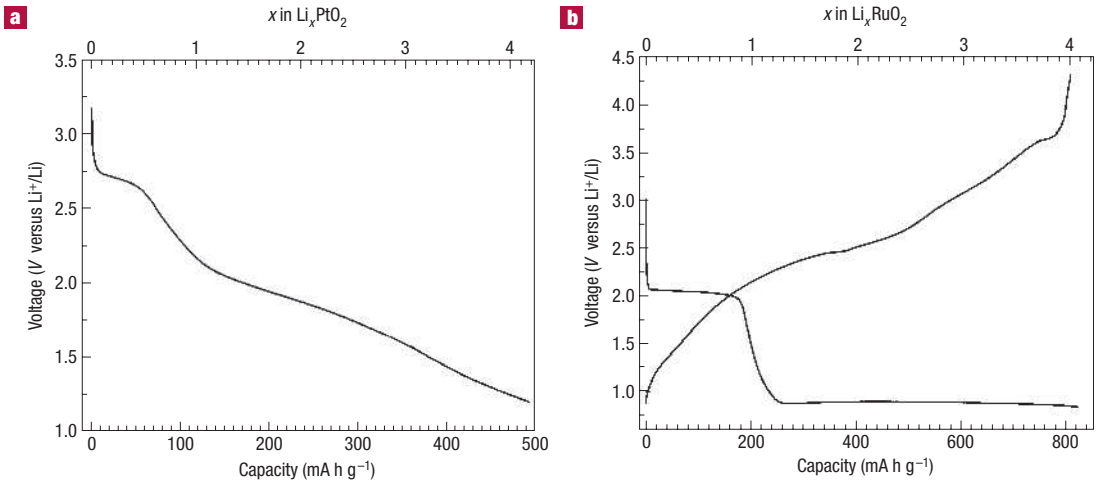

Figure 2 Electrochemical lithiation and delithiation. a, Discharge (Li insertion, voltage decreases) curve of a PtO_2 electrode discharged to 1.2 V. **b**, Discharge and charge (Li extraction, voltage increases) curves of a RuO_2 electrode cycled between 0.8 and 4.3 V.

The overall synthetic procedure is shown in Fig. 1 and the experimental details of the top-down process are described in the Methods section. Here we select two examples to demonstrate the power of the template-free strategy. The first one is the synthesis of nanoporous Pt from submicrometre PtO_2 by electrochemical lithiation followed by dissolving the Li_2O in acidic aqueous solution or even water (Fig. 1):

$$4Li + PtO_2 \rightarrow Pt{:}2Li_2O \quad (1)$$

$$Pt{:}2Li_2O + 4H^+ \rightarrow Pt\ (\text{nanoporous}) + 4Li^+ + 2H_2O.$$

In an electrochemical lithiation process, it is expected that 4Li can be inserted into the starting material of PtO_2, resulting in the formation of the Pt/Li_2O nanocomposite. Figure 2a shows the discharge (Li insertion, voltage decreases) curve of the PtO_2 electrode. The specific discharge capacity is about 490 mA h g^{-1} (4.15Li) and is close to the theoretical capacity of 472 mA h g^{-1} (4Li), accompanied by a volume expansion of up to 100%. To gain better insight into the structure evolution, high-resolution transmission electron microscopy (HRTEM) and selected-area electron diffraction (SAED) were carried out. The particle size of the initial PtO_2 (bottom right inset in Fig. 3a) is in the 0.15−0.30 μm range. In a HRTEM image taken from the edge of a particle (Fig. 3a), the lattice fringes are clearly visible with a spacing of 0.266 nm, which is in good agreement with the spacing of the (100) planes of PtO_2. The corresponding SAED pattern (top left inset in Fig. 3a) also confirms the single-crystal structure of the PtO_2 particle.

On insertion of 4Li, disintegration within the particle is observed (bottom right inset in Fig. 3b), resulting in nanograins of 2–8 nm (Fig. 3b). The lattice fringes with a spacing of 0.226 nm are clearly visible in these nanograins, which is in good agreement with the spacing of the (111) planes of Pt, thus demonstrating the presence of nanocrystalline Pt. The corresponding SAED pattern revealed a set of rings (top left inset in Fig. 3b), which can be indexed as metallic Pt, further demonstrating the occurrence of the lithiation reaction (1). When Li_2O was removed from the Pt/Li_2O nanocomposite by washing in acidic aqueous solution, a nanoporous structure of Pt was obtained. HRTEM and the SAED pattern confirm that the crystallinity of the Pt nanograins was retained but pores of various sizes in the 2–20 nm range were formed (see Supplementary Information, Fig. S1, note that before the HRTEM measurement, the sample was ultrasonicated in ethanol). To further investigate the pore structure of the sample after washing, a nitrogen isothermal adsorption technique was used. Figure 3c shows adsorption/desorption isotherms that exhibit a hysteresis typical of a nanoporous system. According to BET (Brunauer–Emmett–Teller) analysis, a total specific surface area of 142 m^2 g^{-1} is obtained along with a total pore volume of 0.17 cm^3 g^{-1} for a pore diameter less than 20 nm. Considering the bulk density of Pt (1 g Pt corresponds to a volume of 0.047 cm^3), the calculated porosity of the nanoporous Pt is 78%, which is close to the theoretical value (76%) obtained from the sacrificial volume of Li_2O on 4Li insertion. The observed hysteresis confirms that pores with characteristic polymodal size distribution are obtained. This phenomenon had previously been observed in certain carbon materials[21]. The BJH (Barrett–Joyner–Halenda) pore size distribution shown in the inset of Fig. 3c, indicates that the Pt particles have various pore sizes in the range 2–20 nm.

In the fields of electrocatalysis and electrochemical storage, nanoporous materials with high surface area exhibit substantial advantages concerning mass and charge transport by providing shorter effective lengths for both electronic and ionic transport, a higher electrode/electrolyte contact area, and in some cases also interfacial local effects (for example, owing to curvature)[22–24]. Pt and its alloys have been widely used as catalysts in various chemical reactions, especially in direct methanol fuel cells owing to their excellent adsorption and dissociation properties[25–28]. The electrocatalytic activity of our nanoporous Pt for the oxidation of methanol was measured in an electrolyte of 1.0 M methanol in 0.5 M H_2SO_4 by using cyclic voltammograms (CVs). For clarity, only the cycles of 1, 10, 20, 30, 40, 50, 60, 70, 80, 90 and 100 are plotted in Fig. 3d. All of the 100 scan cycles evolved in a similar manner as shown in Fig. S2 in the Supplementary Information. The peak potential for the oxidation of methanol is approximately 0.68 V (versus a saturated calomel electrode), in agreement with the values in the literature[25–28]. The peak current density of the first scan cycle for the nanoporous Pt with a Pt loading of 0.05 mg cm^{-2} is up to 9.3 mA cm^{-2} (that is, the mass current density per unit mass of platinum is 186 mA mg^{-1}). Even after 100 scan cycles the peak current density is still as high as 8.0 mA cm^{-2} (that is,

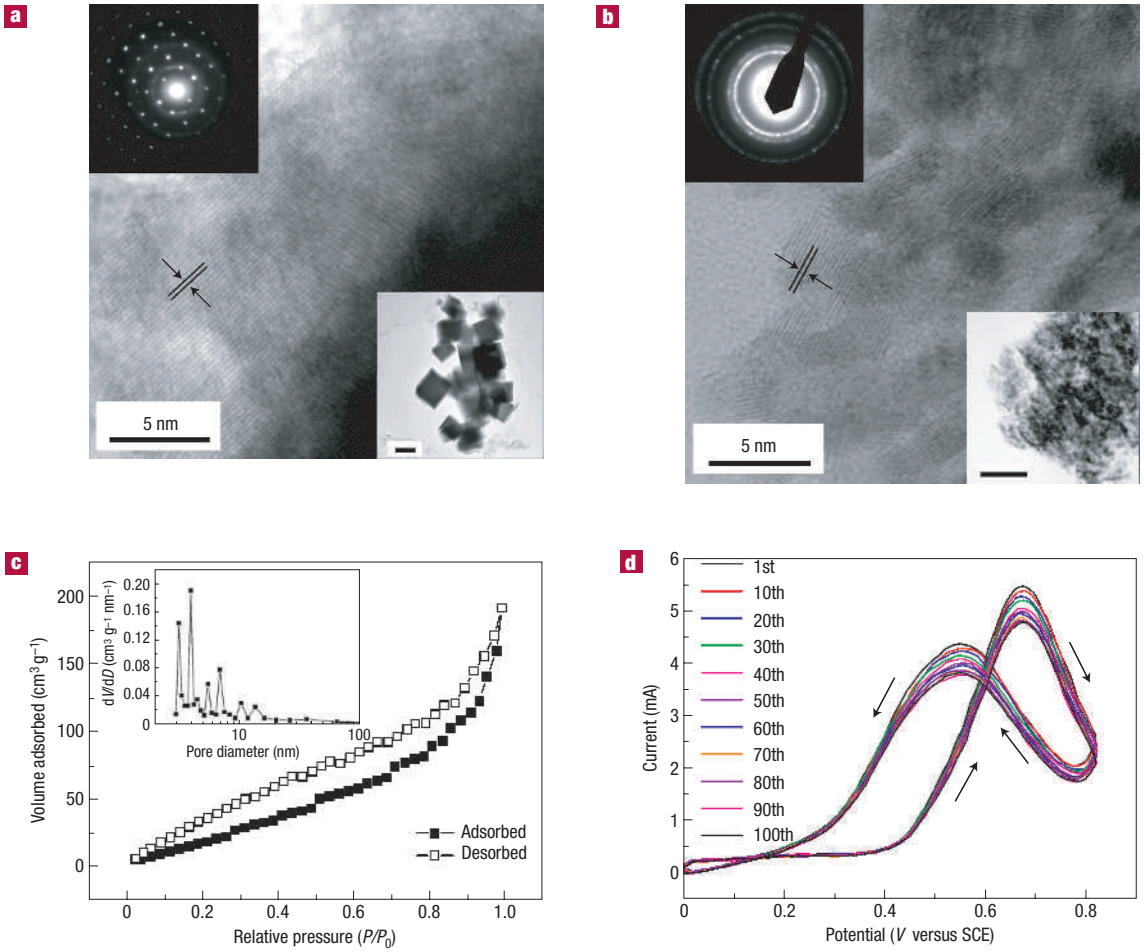

Figure 3 Characterization of nanoporous Pt. a,b, HRTEM images of (**a**) the initial situation—the arrows show the lattice spacing of 0.266 nm, the top left and bottom right insets show the SAED pattern and the overview image of this sample (scale bar, 200 nm); (**b**) discharged to 1.2 V—the arrows show the lattice spacing of 0.226 nm, the top left and bottom right insets show the SAED pattern and the overview image of this sample (scale bar, 30 nm). **c**, Nitrogen adsorption/desorption isotherms of sample (**b**) after washing. Inset: The pore size distribution plot that was calculated by the BJH formula in the adsorption branch isotherm. **d**, Cyclic voltammograms for the nanoporous Pt electrode cycled at a scan rate of 20 mV s^{-1} in 1.0 M methanol in 0.5 M H_2SO_4 solution. The geometric area of the electrode is 0.59 cm^2.

160 mA mg^{-1}). To the best of our knowledge, this nanoporous Pt shows the highest catalytic activity observed for pure Pt mixed in a standard way with carbon as support. Better performance was only achieved by using additional active admixtures, such as Ru or W_2C, which counteract CO poisoning[28]. The experimental result reported here highlights the potential application of nanoporous metallic Pt prepared by the electrochemical lithiation method as a highly efficient catalyst in direct methanol fuel cells.

The present synthesis procedure can also be extended to prepare nanoporous metal oxides. The possibility of this approach has been attested in the second example, namely the preparation of nanoporous RuO_2 from submicrometre RuO_2 by the electrochemical lithiation/delithiation process:

$$4Li + RuO_2 \rightarrow Ru{:}2Li_2O$$

$$Ru{:}2Li_2O \rightarrow RuO_2\ (\text{nanoporous}) + 4Li.$$

For this purpose we first introduce Li (discharging), generating a metal/ Li_2O nanocomposite, then remove it (charging), generating a nanostructured metal oxide (Fig. 1), which is processed further. This process is largely identical to the RuO_2/Li battery cycle described in ref. 15. In the electrochemical lithiation/delithiation process, it can be seen from the discharge and charge curves that 4Li can be reversibly inserted and extracted into and out of RuO_2, resulting in the formation of Ru/Li_2O nanocomposite and nanocrystalline RuO_2, respectively (Fig. 2b) (this is in agreement with ref. 15).

After electrochemical lithiation/delithiation, the HRTEM image (Fig. 4b, inset) reveals a disintegrated but cohesive microstructure which is due to the irreversible volume expansion on Li insertion/extraction, in contrast to the intact single crystal (30 nm−0.2 μm) in its initial stage (Fig. 4a). Disordered nanopores and nanograins of 2–8 nm within the microstructure can be clearly observed in the micrographs. The nanoporous feature was further confirmed by BET investigation (Fig. 4c). The results show a total specific surface area of 239 $m^2 g^{-1}$, 51 $m^2 g^{-1}$ of which can be attributed to micropores and 188 $m^2 g^{-1}$ to mesopores. The total pore volume, if only considering pore diameter less than 20 nm, is 0.20 $cm^3 g^{-1}$, corresponding to a porosity of about 58%. This is close to the theoretical value (50%) obtained from volume expansion (100%) on 4Li insertion. The BJH pore size

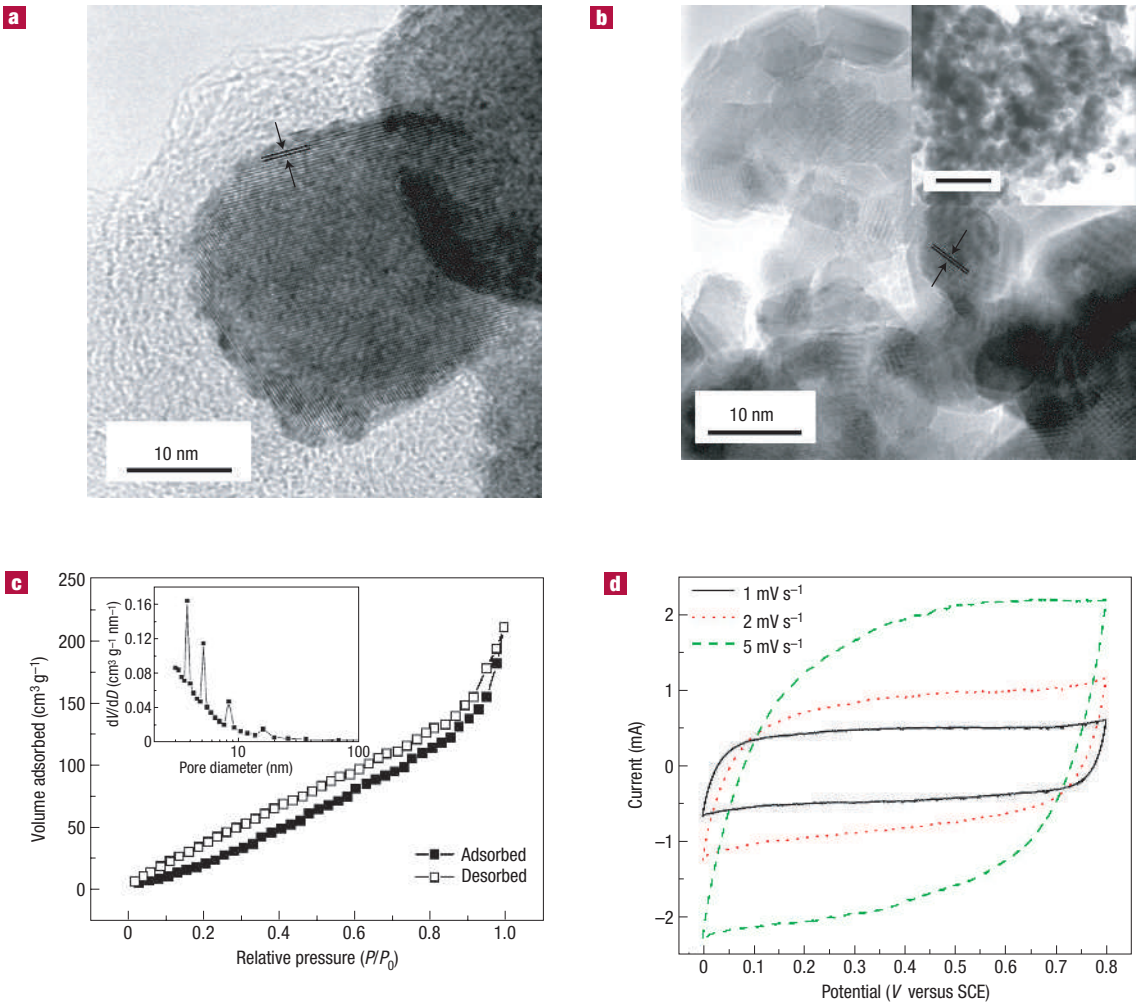

Figure 4 Characterization of nanoporous RuO_2. a,b, HRTEM images of (**a**) the initial situation—the arrows show the lattice spacing of 0.318 nm; (**b**) fully charged (complete Li extraction) to 4.3 V—the arrows show the lattice spacing of 0.256 nm, the inset shows the overview image of this sample (scale bar, 50 nm). **c**, Nitrogen adsorption/desorption isotherms of sample shown in **b**, the inset shows the BJH pore size distribution plot. **d**, Cyclic voltammograms for the nanoporous RuO_2 electrode cycled at different scan rates in 1.0 M H_2SO_4 solution.

distribution shown in the inset of Fig. 4c, indicates that the resulting RuO_2 exhibits various distinguished pore diameters of 3.8, 5.4, 8.2 and 16 nm. The HRTEM image of the sample after immersion into 1.0 M H_2SO_4 solution shows that it still retains its morphology and pore structure (see Supplementary Information, Fig. S3). The micro-Raman spectra also reveal the nanocrystalline RuO_2 structure (see Supplementary Information, Fig. S4), again indicating that the nanoporous RuO_2 is stable in water or in acid solution.

Owing to the high surface area, the presence of various pore sizes and the pronounced stability of the nanoporous RuO_2, it is expected to exhibit excellent supercapacitive performance. The typical CVs recorded at different scan rates for the nanoporous RuO_2 electrode in 1.0 M H_2SO_4 solution are shown in Fig. 4d. The mirror-like profile of the CV curves indicates a high reversibility as observed in previous cases[19,20]. The specific capacitance calculated by the mass of RuO_2 was found to be about 385 F g^{-1} at a scan rate of 1 mV s^{-1}. At higher scan rates of 2 and 5 mV s^{-1}, capacitance values of about 350 and 292 F g^{-1} were obtained. A decrease in capacitance at higher scan rates is a common phenomenon[19,20], however, the specific capacitance of the nanoporous RuO_2 is close to three hundred times larger than that of the starting RuO_2 (1.2 F g^{-1}) (see Supplementary Information, Fig. S5). This value is also six times larger than that of mesoporous RuO_2 synthesized by the soft templating method[20]. Higher values of specific capacitance have only been achieved in hydrated ruthenium oxide ($RuO_2 \cdot 0.5H_2O$) in which water is incorporated into the bulk[19]. An excellent cycling performance at a scan rate of 5 mV s^{-1} was also obtained (see Supplementary Information, Fig. S6) for the nanoporous RuO_2. The main reason for the remarkably improved performance of the present nanoporous RuO_2 is attributed to the high surface area and the special pore size distribution.

In conclusion, the electrochemical synthesis based on previous experience in Li batteries[13–18] opens a new path for the template-free room-temperature fabrication of well-crystallized materials with favourable nanostructure and superior chemical or electrochemical properties. The synthetic procedure is relatively simple (starting from micrometre-sized transition metal oxides), yet very effective, and owing to its versatility, can also be extended to the synthesis of other nanostructured transition metal oxides and also to sulphides, fluorides, chlorides, nitrides and phosphides[14,16,17,23,29,30]. The procedure is not restricted to noble metals or noble metal

compounds[18]. Ongoing work shows the possibility of successfully preparing nanoporous crystalline Ni, Co, Fe using water as the solvent for Li_2O. Other anions such as sulphide or chloride might be used to prepare even more reducing metals, as Li_2S or LiCl formed *in situ* can be removed by organic solvents (for example, ethanol or propylene carbonate). In addition, structure-forming chemical agents other than Li (Na, Mg and so on) and varied electrochemical conditions might be used to achieve different pore structures and size distributions. We anticipate that nanoporous materials with increasingly rich inorganic compositions will make a decisive impact in future applications in various fields such as electrochemical storage, electrocatalysts, photocatalysts and sensors. As they, on one hand, are of high significance for electrochemical devices or as catalysts, and as, on the other hand, nanoporous materials are pronouncedly non-equilibrium structures, it is the design of tailored preparation procedures such as that described here which will determine the rate of progress in this area.

METHODS

Electrochemical lithiation/delithiation experiments were carried out using a two-electrode Swagelok-type cell. To prepare working electrodes, a mixture of PtO_2 (Aldrich) or RuO_2 (Alfa) and poly(vinyl difluoride), at a weight ratio of 90:10, was pasted on pure Ni foil/mesh. Experiments for electrocatalytic and supercapacitive performances were conducted on the electrode composed of PtO_2/RuO_2, carbon black and poly(vinyl difluoride) (5:90:5/50:45:5). Glass fibre (GF/D) from Whatman was used as a separator. Pure lithium foil (Aldrich) was used as a counter electrode. The electrolyte consists of a solution of 1 M $LiPF_6$ in ethylene carbonate/dimethyl carbonate (1:1 by volume) obtained from Ube Industries. The cell was assembled into a three-layered structure (PtO_2/RuO_2, glass fibre and lithium foil) in an argon-filled glove box. A discharge and charge test at a rate of C/10 was carried out on an Arbin MSTAT system. Before the following measurements, the samples were washed with dimethyl carbonate in air to remove the residual electrolyte and dried under vacuum at room temperature. Micro-Raman spectra were recorded on a Jobin Yvon LabRam spectrometer using a 632.8 nm excitation laser line. HRTEM was carried out on a JEOL 4000EX transmission electron microscope, operating at 400 kV. Before HRTEM measurements, the sample was ultrasonicated in ethanol. The nitrogen sorption isotherms were obtained with an Autosorb-1 system (Quanta Chrome); the sample after electrochemical lithiation/delithiation was outgassed overnight at 100 °C before the measurements. Electrocatalytic and supercapacitive performances were characterized with a three-electrode configuration, where a platinum foil, SCE and Pt/RuO_2 electrode were used as counter, reference and working electrodes, respectively. 1.0 M methanol in 0.5 M H_2SO_4 solution and 1.0 M H_2SO_4 solution were used as electrolytes for the electrocatalytic and supercapacitive measurements, respectively. The electrolyte was purged with nitrogen gas for 30 min before the electrochemical measurements. Cyclic voltammograms were carried out on a Solartron SI 1287 electrochemical interface.

Received 10 February 2006; accepted 16 June 2006; published 13 August 2006.

References

1. Davis, M. E. Ordered porous materials for emerging applications. *Nature* **417,** 813–821 (2002).
2. Corma, A. From microporous to mesoporous molecular sieve materials and their use in catalysis. *Chem. Rev.* **97,** 2373–2419 (1997).
3. Joo, S. H. *et al.* Ordered nanoporous arrays of carbon supporting high dispersions of platinum nanoparticles. *Nature* **412,** 169–172 (2001).
4. Scott, B. J., Wirnsberger, G. & Stucky, G. D. Mesoporous and mesostructured materials for optical applications. *Chem. Mater.* **10,** 3140–3150 (2001).
5. Bronstein, L. M., Weissenberger, M. C. & Antonietti, M. Mesoporous alumina and aluminosilica with Pd and Pt nanoparticles: structure and catalytic properties. *Chem. Mater.* **15,** 2623–2631 (2003).
6. Kresge, C. T., Leonowicz, M. E., Roth, W. J., Vartuli, J. C. & Beck, J. S. Ordered mesoporous molecular-sieves synthesised by a liquid-crystal template mechanism. *Nature* **359,** 710–712 (1992).
7. Yang, P. D., Zhao, D. Y., Margolese, D. I., Chmelka, B. F. & Stucky, G. D. Generalized syntheses of large-pore mesoporous metal oxides with semicrystalline frameworks. *Nature* **396,** 152–155 (1998).
8. Grosso, D. *et al.* Periodically ordered nanoscale islands and mesoporous films composed of nanocrystalline multimetallic oxides. *Nature Mater.* **3,** 787–792 (2005).
9. Deshpande, A. S., Pinna, N., Smarsly, B., Antonietti, M. & Niederberger, M. Controlled assembly of preformed ceria nanocrystals into highly ordered 3D nanostructures. *Small* **1,** 313–316 (2005).
10. Ba, J. H., Polleux, J., Antonietti, M. & Niederberger, M. Non-aqueous synthesis of tin oxide nanocrystals and their assembly into ordered porous mesostructures. *Adv. Mater.* **17,** 2509–2512 (2005).
11. Ying, J. Y., Mehnert, C. P. & Wong, M. S. Synthesis and applications of supramolecular-templated mesoporous materials. *Angew. Chem. Int. Edn* **38,** 56–77 (1999).
12. Wu, Y. Y. *et al.* Composite mesostructures by nano-confinement. *Nature Mater.* **3,** 816–822 (2004).
13. Poizot, P., Laruelle, S., Grugeon, S., Dupont, L. & Tarascon, J.-M. Nano-sized transition metal oxides as negative material for lithium-ion batteries. *Nature* **407,** 496–499 (2000).
14. Poizot, P., Laruelle, S., Grugeon, S. & Tarascon, J.-M. Rationalization of low-potential reactivity of 3d-metal-based inorganic compounds toward Li. *J. Electrochem. Soc.* **149,** A1212–A1217 (2002).
15. Balaya, P., Li, H., Kienle, L. & Maier, J. Fully reversible homogeneous and heterogeneous Li storage in RuO_2 with high capacity. *Adv. Funct. Mater.* **13,** 621–625 (2003).
16. Badway, F., Cosandey, F., Pereira, N. & Amatucci, G. G. Carbon metal fluoride nanocomposites—High-capacity reversible metal fluoride conversion materials as rechargeable positive electrodes for Li batteries. *J. Electrochem. Soc.* **150,** A1318–A1327 (2003).
17. Li, H., Balaya, P. & Maier, J. Li-storage *via* heterogeneous reaction in selected binary metal fluorides and oxides. *J. Electrochem. Soc.* **151,** A1878–A1885 (2004).
18. Zhang, D. W., Chen, C. H., Zhang, J. & Ren, F. Novel electrochemical milling method to fabricate copper nanoparticles and nanofibers. *Chem. Mater.* **17,** 780–785 (2005).
19. Long, J. W., Swider, K. E., Merzbacher, C. I. & Rolison, D. R. Voltammetric characterization of ruthenium oxide-based aerogels and other RuO_2 solids: The nature of capacitance in nanostructured materials. *Langmuir* **15,** 780–785 (1999).
20. Subramanian, V., Hall, S. C., Smith, P. H. & Rambabu, B. Mesoporous anhydrous RuO_2 as a supercapacitor electrode material. *Solid State Ion.* **175,** 511–515 (2004).
21. Polarz, S., Smarsly, B. & Schattka, J. H. Hierachical porous carbon structures from cellulose acetate fibers. *Chem. Mater.* **14,** 2940–2945 (2002).
22. Maier, J. Nanoionics: Ion transport and electrochemical storage in confined systems. *Nature Mater.* **5,** 805–815 (2005).
23. Arico, A. S., Bruce, P. G., Scrosati, B., Tarascon, J.-M. & Schalkwijk, W. V. Nanostructured materials for advanced energy conversion and storage devices. *Nature Mater.* **4,** 366–376 (2005).
24. Schoonman, J. Nanostructured materials in solid state ionics. *Solid State Ion.* **135,** 5–19 (2000).
25. Carrette, L., Friedrich, K. A. & Stimming, U. Fuel cells: principles, types, fuels, and applications. *ChemPhysChem* **1,** 162–193 (2000).
26. Che, G., Lakshmi, B. B., Fisher, E. R. & Martin, C. R. Carbon nanotubule membranes for electrochemical energy storage and production. *Nature* **393,** 346–349 (1998).
27. Guo, Y.-G. *et al.* Tin/platinum bimetallic nanotube array and its electrocatalytic activity for methanol oxidation. *Adv. Mater.* **17,** 746–750 (2005).
28. Ganesan, R. & Lee, J. S. Tungsten carbide microspheres as a noble-metal-economic electrocatalyst for methanol oxidation. *Angew. Chem. Int. Edn* **44,** 6557–6560 (2005).
29. Pereira, N., Dupont, L., Tarascon, J.-M., Klein, L. C. & Amatucci, G. G. Electrochemistry of Cu_3N with lithium—a complex system with parallel processes. *J. Electrochem. Soc.* **150,** A1273–A1280 (2003).
30. Gillot, F. *et al.* Electrochemical reactivity and design of NiP_2 negative electrodes for secondary Li-ion batteries. *Chem. Mater.* **17,** 6327–6337 (2005).

Acknowledgements

The authors are indebted to the Max Planck Society and acknowledge support in the framework of the ENERCHEM project. The authors thank P. Kopold, A. Schulz and A. Fuchs for their technical support and H. Li and L. Z. Fan for helpful discussions.
Correspondence and requests for materials should be addressed to Y.-G.G. or J.M.
Supplementary Information accompanies this paper on www.nature.com/naturematerials.

Competing financial interests

The authors declare that they have no competing financial interests.